Initial Test of a Stirling Cryocooler with a High Cooling Capacity

G.Y.Yu[1,2], W.Dai[1], J.Qiu[2], L.M.Zhang[1], X.W.Li[1,3], B.Liu[2], Z.H.Wu[1], J.Y.Xu[1,3], E.C.Luo[1], H.B. Li[2]

[1]Key Laboratory of Cryogenics, Technical Institute of Physics and Chemistry, Chinese Academy of Sciences, Beijing, 100190 China
[2]Zhongke Lihan (Shenzhen) Thermo-acoustic Technology Inc., Shenzhen 518055, China
[3]University of Chinese Academy of Sciences, Beijing 100049, China

ABSTRACT

Cryocoolers with a high cooling capacity around 80 K~120 K may find important application in boil-off gas recondensation and power applications for high temperature superconductors. Among the cryocoolers, the free piston Stirling cryocooler (FPSC) is a good candidate due to its attractive virtues of compact size and high thermal efficiency. In this work, a FPSC has been designed based on our previous optimization with thermo-acoustic theory. The configuration was further studied through computational fluid dynamics (CFD) software. Moreover, an experimental system was built for validation of the predictions. Preliminary experiments were carried out to study the fundamental performance in terms of the cool-down characteristics, the temperature distribution, the cooling power and thermal efficiency. The coupling between the FPSC and the linear compressor was also briefly discussed. A cooling power of 56 W was obtained at 80 K with a charge pressure of 3 MPa of helium and a operating frequency of 50 Hz. The relative Carnot efficiency of the FPSC in terms of input acoustic power was 16.4%.

INTRODUCTION

The free piston Stirling cryocooler has evolved to be a very promising technology since its debut in the 1980s [1]. Due to its remarkable features of high reliability, high thermal efficiency and high specific power (cooling power per unit volume), FPSC has been used in cooling devices in civil and aerospace applications [2]. The typical cooling capacity is around 10 W at 80 K. The recent boom in boil-off gas recondensation and power application of superconductor sparks enthusiasm for FPSC with large cooling power (100 W to kilowatt) at liquid nitrogen temperature [3]. In 2011, Karandikar et al. [4] reported their design concept of an FPSC which offered 100 W at 65 K with an input power of 2.2 kWe. The overall efficiency (cooling power/input electric power) of the optimized FPSC can reach 4.5%, as comparabled to their 5 W FPSC counterparts [4]. However, there are no further reports on their test results to date. As a leading company in the field of free piston Stirling engine, Inifinia has made attempts to develop their prototypes with an innovative double-acting configuration [5].

Cryocoolers 18, edited by S.D. Miller and R.G. Ross, Jr.

In our previous work [6], the intrinsic physical mechanism of an FPSC has been clearly analyzed from the perspective of thermo-acoustic theory. According to our optimization results, an FPSC could provide about 300 W at 80 K corresponding to a relative Carnot efficiency of 48% (compressor not included) when it is well designed. In order to validate the design, CFD simulation and preliminary experiments were carried out in this work. Our recent research is introduced in this paper. The design details and CFD simulation against the calculation based on linear thermo-acoustic theory will first be introduced. Then, based upon our calculations, an experimental setup was built and tested which will be presented. Lastly, some discussions are given of this work.

DESIGN DETAILS AND CFD SIMULATION

Design Details

As generally understood in thermo-acoustics, FPSC and Stirling-type pulse tube cooler (SPTC) can all be group into thermo-acoustic systems. Therefore, the basic design principles of these two cryocoolers are exactly the same except for their distinct phase shifting mechanism. In this section, we will first introduce the detailed configuration of an FPSC which is based upon our years of experiences in coaxial Stirling type pulse cooler (SPTC) [7].

Table 1 gives our design parameters of an FPSC. The layout of the FPSC is shown in Figure 1. In the experiments, a dual opposed linear compressor, CFIC 2S241W, is used to drive the cold head. The FPSC includes the regenerator, heat exchangers (HX), displacer, expansion space and compression space. Obviously, the heat exchangers and regenerator are located outside in the annular space around the displacer which is put in the center with flexure bearings inside its hollow body. This arrangement not only results in the convenience of assembling, but also sets the benchmark for future improvement.

Table 1. Main dimension and configuration of an FPSC in series

Components	Details
Compression space	Roughly 300 ml
Ambient HX	35 mm long, with roughly 30% porosity, 0.4 mm gas channel width
Regenerator	6 cm long, equivalent i.d. 9 cm, filled with 300# stainless steel mesh
Cold HX	30 mm long, with roughly 25% porosity, 0.3 mm gas channel width
Expansion space	Roughly 45 ml
Displacer	75 mm diameter facing the cold side, rod diameter 25 mm, equivalent moving mass 1.19 kg, spring constant 100 kN/m, nominal mechanical resistance around 30 Ns/m

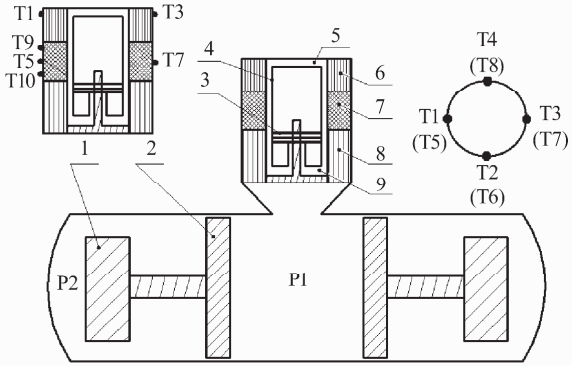

Figure 1. Schematic of the FPSC with linear compressor included, where 1 is the CFIC STAR linear motor, 2 is the piston, 3 is the flexure bearings, 4 is the displacer, 5 is the expansion space, 6 is the cold HX, 7 is the regenerator, 8 is the ambient HX, and 9 is the compression space.

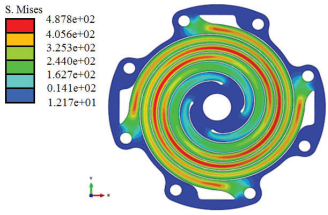

Figure 2. Profile and stresses of the displacer flexure bearing

For the ambient HX and cold HX, a plate-fin type heat exchanger which is manufactured through EDM is used to ensure flow uniformity and good heat transfer between the working gas and the solids. To carry the heat away, cooling water is flowing through a stainless steel water jacket in which the copper ambient HX is located. Constantan wires heated by a direct-voltage source are wound circumferentially on the surface of the cold HX to simulate the cooling load. As the key part of the thermodynamic core, the regenerator requires perfect heat transfer between the oscillating gas and the solids as well as a small flow resistance. Through careful calculation, 300-mesh stainless steel screens are chosen which has a good balance between the heat transfer and the flow loss. In order to eliminate the axial leakage within the regenerator due to the mismatch between the machined screen and the housing walls, a slight axial compression and interference fit is used.

The displacer is located in the center of the setup. Flexure bearings are used to provide the axial spring force required for the moving mass. The flexure profiles are developed in ProE and then optimized in Abacus. The design target is to obtain the desired axial spring rates and minimize the stress intensity within the flexure. The predicted axial and radial spring rates of the displacer flexure are 100 kN/m and 450 kN/m, respectively. The profile and the stress results are shown in Fig. 2. This stress level is obtained when the amplitude of the displacement reaches 6 mm, 50% above the design value of 4 mm. Fortunately, the maximum stress intensity is below the mean endurance limit of the spring material. These flexure bearings are capable of operating at 50 Hz with a greater resonant frequency.

CFD Simulation

As stated earlier [8], thermo-acoustic theory has shed new light on the mechanisms of the FPSC and provided a new design tool. However, this linear and quasi-1D tool is incapable of accomodating the influence of multi-dimensional and time-dependent turbulence effects, which might consequently cause divergence between the calculations and the experiments. A CFD simulation has been conducted prior to the experiments. The CFD simulation has been proven to be a powerful tool to study the complicated flow and heat transfer in the regenerative cryocoolers [9]. Herein, the commercially available codes FLUENT was used.

Given the purpose of the CFD simulation, emphasis was placed on the simulation results and the modeling efforts, including the geometry modeling, mathematical model, initial and boundary condition, and numerical scheme. Table 2 lists these simulation parameters [10]. In addition, dynamic mesh model has been used to mimic the oscillatory movement of the piston and displacer. The velocities of the piston and displacer are defined as follows.

$$u_{piston} = \omega X_{piston} \cos(\omega t) \tag{1}$$

$$u_{displacer} = \omega X_{displacer} \cos(\omega t + \theta) \tag{2}$$

where X is the displacement amplitude, ω is the angular frequency and θ is the phase difference between the piston and the displacer. It should be noted that for simplicity, the movement of the displacer is specified throughout the simulation which is quite inconsistent with the practical operation where the movement of the displacer is determined passively by the forces upon it. The benefit is appreciable because of the time- saving. In this simulation, the displacement of the piston and displacer as well as their phase difference is assigned to be 9.6 mm, 3.2 mm and 46.8 degree, respectively. Another important issue that should be stated is that, in order to appreciably reduce

the computation time, only 1/200 of the whole FPSC has been modeled which implies that only one complete fin and adjacent flow channel of the HXs would be modeled and simulated. In this calculation, a fixed time step of 2.5×10^{-5} s is found to be sufficient to produce results independent of time step size. A mesh of 10, 0000 nodes is chosen for the simulation. Figure 3 displays the meshed model.

Typical results when the calculation reaches quasi-steady state are illustrated in Figs 4 - 6. Figure 4 shows the transient contour of the temperature. A linear temperature distribution could be apparently captured axially across the regenerator. It is not surprising that temperature inhomogeneity occurs in the adjoining parts due to the abrupt change in the cross-sectional areas. The same homogeneity is also found in the contour of the dynamic pressure as displayed in Figure 5. In contrast to the distribution of temperature and dynamic pressure, the contours of cyclic-averaged X-direction velocity and Y-direction velocity shown in Figure 6 are rather complicated. Flow vortices could be readily detected in both the compression and expansion spaces, especially the compression space where strong mixing of three streams of gas happens. Vortices in the ends of the ambient HX indicate that flow straightener may be needed to smooth the flow therein.

Table 3 shows the comparison between the CFD simulations and calculations based on self-developed linear thermo-acoustic program. The good agreement on the pressure amplitudes is not surprising given the same assigned movements of the moving parts. With the most concerned items, i.e., the input acoustic power and the cooling power, the discrepancy is a bit larger than expected. One possibility is that the dissipation mechanism related to the multi-dimensional effects is considered in the CFD simulation. Another possibility as found in our previous computations, is that it's rather time consuming for the items involving several single variables, such as acoustic work and cooling power to reach the final steady state. From the trend of simulation, this discrepancy might narrow.

Table 2. Numerical model details in the CFD simulation

Settings	Detail
Solver	Unsteady, double precision,
Sub-model	Porous media for HXs and regenerator, RNG k-epsilon turbulence model
Initial conditions	3.0 MPa helium, 298 K for the ambient HX, 80 K for the cold HX
Boundary conditions	Adiabatic thermal conditions for all the walls except for the those of HXs
Numerical Scheme	1st-order implicit time differencing 2nd-order upwind differencing for the continuity, momentum and energy equations PISO pressure-velocity coupling

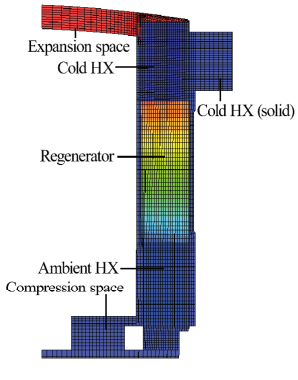

Figure 3. Schematic of the meshed model

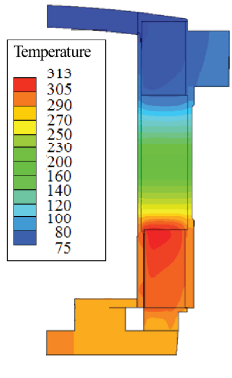

Figure 4. Transient contour of the temperature

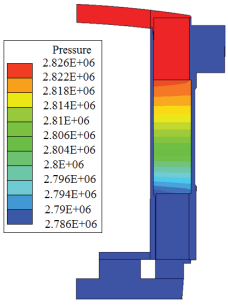

Figure 5. Transient contour of the dynamic pressure

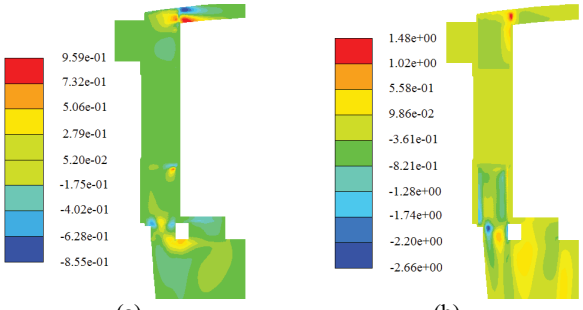

Figure 6. Contour of the cyclic-averaged X-direction and Y-direction velocity. (a) X-direction, (b) Y-direction

Table 3. Comparison between CFD and thermo-acoustic calculation

	Pressure amplitude at P1 (MPa)	Input acoustic power (W)	Cooling power (W)
CFD	0.313	1907	210.5
Thermo-acoustic	0.319	1684	248.5

EXPERIMENTS

The experimental setup was built and tested accordingly. The FPSC is instrumented with several pressure sensors and calibrated Pt-100 resistance thermometers with an accuracy of 0.1 K. As shown in Figure 1, the pressure sensors are located in the backside volume and outlet of the linear compressor, respectively. Four thermometers are located equidistantly around the cold HX. Another four are located on the circumference of the regenerator at roughly half of its length to measure the azimuthal temperature distribution. The last two are also located along the axis of the regenerator equidistantly to measure the longitudinal temperature distribution. The input electric power is determined by voltage and current measurements. For all the experiments, the FPSC is vertically positioned with the cold HX on top.

Besides the cooling down and temperature distribution characteristic seen in Figures 7 and 8, another issue concerned is the cooling power and the thermal efficiency seen in Table 4. Generally speaking, the more the input acoustic power, the larger the cooling power. Therefore, an effective way to increase the cooling power is to enlarge the input acoustic power. However, due to assembly problems, the displacement of the displacer is confined to about 3.5 mm, which presents a big obstacle to increasing the input acoustic power. With 933 W of input acoustic power, the cooling power is 56 W, corresponding to a relative Carnot efficiency of 16.4%. The agreement between the measured results and predicted results based on thermo-acoustic program in Table 4 is fairly poor. The reasons for this huge discrepancy include an apparently poor quality of the displacer assembly, and, over-estimated heat transfer in the cold HX in calculation, etc. All these factors are under further investigation.

On a system level, the efficiency of the linear compressor is of equivalent significance. In the experiments the efficiency of the compressor is as low as ~46%, indicating a disappointing overall efficiency. The main reason is that the CFIC compressor is temporarily used to investigate the performance of the cold head and mismatch between the compressor and the cold head exists. By adjusting the void volume between the compressor and the FPSC, the match could be somewhat improved. Specially-designed compressors will be provided by Zhong Ke Li Han Inc. in the future.

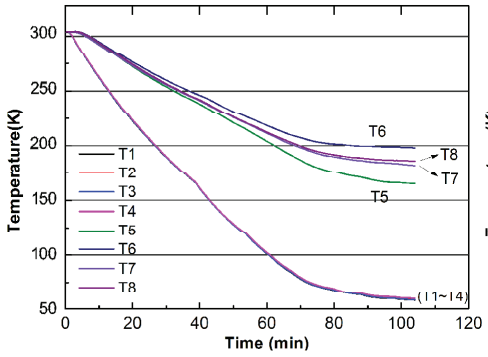

Figure 7. Typical cooling down curve

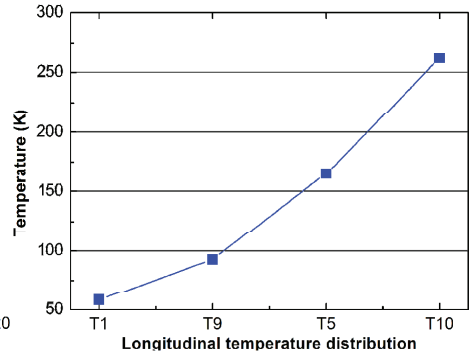

Figure 8. Longitudinal temperature distribution

Table 4. Comparison between experiment and thermo-acoustic calculation, 3.0 MPa helium, pressure amplitude of 0.27 MPa at P1, frequency of 50 Hz

	Input acoustic power (W)	Cooling power (W)
Experiment	933	56
Thermo-acoustic	1116	128

CONCLUSION

This work described the design details of an FPSC with expected high cooling capacity at 80 K. Prior to experiments, CFD simulation has been conducted and a comparison to the calculation with thermo-acoustic theory shows reasonable agreement. The deviation indicates that the multi-dimensional and turbulence effect should be carefully taken into consideration. The preliminary experimental results have shown a relative Carnot efficiency of 16.4% (cooling power/acoustic power) with the cooling power of 56 W at 80 K. So far, there are some mechanical, flow and heat transfer problems that need to be deeply studied and overcome. With these improvements and better understanding of the system, a marginal performance improvement in terms of both FPSC and overall efficiency are expected in the future.

ACKNOWLEDGMENT

This work is financially supported by the Natural Science Foundation of China with Grant No. 11004206 and the Youth Innovative Society of Chinese Academy of Sciences.

REFERENCE

1. http://www.sunpowerinc.com/cryocoolers/cryotel.php
2. Robert, B. "On-bit performance of the RHESSI cryocooler," *Cryogenics,* Vol. 44 (2004), pp. 389-393.
3. Ganni, V., Fesmire, J.E., "*Cryogenics for superconductors: refrigeration, delivery, and preservation of the cold*," *Adv. in Cryogenic Engineering*, Vol. 57, Amer. Institute of Physics, Melville, NY (2012), pp. 15-27.
4. Karandikar, A., and Fiedler, A., *"Scaling STI's sapphire cryocooler for applications requiring higher heat loads"*, *Adv. in Cryogenic Engineering*, Vol. 57, Amer. Institute of Physics, Melville, NY (2012), pp. 675-682.
5. http://www.superconductivityiea.org/document/M.%20White%20Infinia%20%20Cryocoolers%20for%20HTS.pdf

6. Yu, G.Y., Li, K., Dai, W., et al. *"*Investigation on a Free Piston Stirling Cryocooler with Large Cooling Capacity*," Adv. in Cryogenic Engineering*, Vol. 59, Amer. Institute of Physics, Melville, NY (2014), pp.1626-1632.

7. Hu, J.Y., Zhang, L.M., Zhu, J., et al. *"*A high-efficiency coaxial pulse tube cryocooler with 500 W cooling capacity at 80 K,*" Cryogenics*, Vol. 62 (2014), pp. 7-10.

8. Dai, W., Yu, G.Y., Xiao, C., et al. *"*Theoretical and experimental investigation of a 1 kWe class free piston Stirling generator,*" The 15th International Stirling Engine Conference*, Sept. 10-22, 2012, Dubrovnik, Croatia.

9. Dion. S., Bakhtier. F.. *"*Wave-shaping of pulse tube cryocooler components for improved performance,*" Cryogenics*, Available online March 13, 2014.

10. Guoyao Y., Dai, W., Luo, E., *"*CFD simulation of a 300 Hz thermoacoustic standing wave engine,*" Cryogenics,* Vol. 50 (2010), pp. 615-622.